HAL open science

Flexible multivariate hemodynamics fMRI data analyses and simulations with PyHRF

Thomas Vincent, Solveig Badillo, Laurent Risser, Lotfi Chaari, Christine Bakhous, Florence Forbes, Philippe Ciuciu

To cite this version:

Thomas Vincent, Solveig Badillo, Laurent Risser, Lotfi Chaari, Christine Bakhous, et al.. Flexible multivariate hemodynamics fMRI data analyses and simulations with PyHRF. Frontiers in Neuroscience, 2014, Brain Imaging methods (eCollection 2014), 8 (Article 67), pp.23. 10.3389/fnins.2014.00067 . hal-01084249

HAL Id: hal-01084249

https://inria.hal.science/hal-01084249

Submitted on 18 Nov 2014

HAL is a multi-disciplinary open access archive for the deposit and dissemination of scientific research documents, whether they are published or not. The documents may come from teaching and research institutions in France or abroad, or from public or private research centers.

L'archive ouverte pluridisciplinaire **HAL**, est destinée au dépôt et à la diffusion de documents scientifiques de niveau recherche, publiés ou non, émanant des établissements d'enseignement et de recherche français ou étrangers, des laboratoires publics ou privés.

Distributed under a Creative Commons Attribution 4.0 International License

Frontiers in Neuroinformatics

Research Article
12 February 2014

Flexible multivariate hemodynamics fMRI data analyses and simulations with PyHRF

Thomas Vincent [1,2], **Solveig Badillo** [2], **Laurent Risser**[2,3], **Lotfi Chaari** [1,4], **Christine Bakhous** [1], **Florence Forbes** [1] **and Philippe Ciuciu** [2,*]

[1] *INRIA, MISTIS, Grenoble University, LJK, Grenoble, France*
[2] *CEA/DSV/I^{2}BM NeuroSpin center, Bât. 145, F-91191 Gif-sur-Yvette, France*
[3] *CNRS, Toulouse Mathematics Institute, UMR 5219, Toulouse, France*
[4] *INP-ENSEEIHT / CNRS UMR 5505, University of Toulouse, IRIT, Toulouse, France*

Correspondence*:
Philippe Ciuciu
CEA/DSV/I^{2}BM NeuroSpin center, Bât. 145, F-91191 Gif-sur-Yvette, France,
philippe.ciuciu@cea.fr

Research Topic

ABSTRACT

As part of fMRI data analysis, the `pyhrf` package provides a set of tools for addressing the two main issues involved in intra-subject fMRI data analysis: (i) the localization of cerebral regions that elicit evoked activity and (ii) the estimation of the activation dynamics also referenced to as the recovery of the Hemodynamic Response Function (HRF). To tackle these two problems, `pyhrf` implements the Joint Detection-Estimation framework (JDE) which recovers parcel-level HRFs and embeds an adaptive spatio-temporal regularization scheme of activation maps. With respect to the sole detection issue (i), the classical voxelwise GLM procedure is also available through `nipy`, whereas Finite Impulse Response (FIR) and temporally regularized FIR models are implemented to deal with HRF estimation concerns (ii). Several parcellation tools are also integrated such as spatial and functional clustering. Parcellations may be used for spatial averaging prior to FIR/RFIR analysis or to specify the spatial support of the HRF estimates in the JDE approach. These analysis procedures can be applied either to volumic data sets or to data projected onto the cortical surface. For validation purpose, this package is shipped with artificial and real fMRI data sets, which are used in this paper to compare the outcome of the different available approaches. The artificial fMRI data generator is also described to illustrate how to simulate different activation configurations, HRF shapes or nuisance components. To cope with the high computational needs for inference, `pyhrf` handles distributing computing by exploiting cluster units as well as multiple cores computers. Finally, a dedicated viewer is presented, which handles n-dimensional images and provides suitable features to explore whole brain hemodynamics (time series, maps, ROI mask overlay).

Keywords: medical imaging analysis, fMRI, Bayesian inference, python, scientific computing

1 INTRODUCTION

As Magnetic Resonance Imaging (MRI) is a growing imaging modality in neuroscience, the need for powerful tools to explore the increasing amount of data is more and more significant. This data growth is quantitative as cohort sizes are getting bigger through the development of international multi-centre projects like the Human Brain Project **Koslow and Huerta** (2013) but also qualitative as high field magnets become more and more available **Duyn and Koretsky** (2011). Functional MRI (fMRI) especially benefits from these improvements and the experimenter has access to finer spatial ($\sim$ 1 mm) and temporal ($\sim$ 1 sec.) resolutions and also higher signal-to-noise ratio (SNR). In particular, the higher temporal resolution combined with higher SNR allows a better recovery of dynamical processes so that we no longer have to accommodate with only static mappings of cerebral activity. In this context, `pyhrf` aims at extracting dynamical features from fMRI data and especially the Blood Oxygenated Level Dependent (BOLD) modality (**Ogawa et al.** (1990)). The observed BOLD signal is an indirect measure of the neural activity via the oxygen variation induced by the neuro-vascular coupling. Therefore, analysis methods have to formalize a hemodynamic model in order to make inference on neural processes. However, even if BOLD variations are known to correlate with neural activity, it is difficult to disentangle the neural and the vascular components in terms of dynamics. As the employed methodology mainly resorts to linear systems, dynamical processes are summarized within the so-called Hemodynamic Response Function (HRF), which is the impulse response that links neuronal stimulation to the fMRI signal, through the neuro-vascular coupling. In fact, the package offers various tools to analyze evoked fMRI data ranging from spatial mappings such as those provided by the General Linear Model (GLM) framework (**Friston et al.** (1995)) to finer hemodynamics models as provided by the joint detection-estimation (JDE) approach described in **Makni et al.** (2005, 2008); **Vincent et al.** (2010). Through a bilinear and time-invariant system, the JDE approach models an unknown Hemodynamic Response Function (HRF) at the level of a group of voxels (termed a parcel in the following) as well as voxel- and condition-specific response levels to encode the local magnitudes of this response. The HRF is only constrained to be smooth (temporal regularization) and can cover a wide variety of shapes. The response levels are spatially regularized within each parcel. Hence, the JDE approach is a spatially adaptive GLM built on an unknown parcel-dependent HRF with spatio-temporal regularization.

The usage of each tool amounts to a model choice which is driven by the features required by the experimenter's questioning. If one is only interested in obtaining classical detection results where the canonical HRF embodies a standard and widely recognized choice, a GLM based on this canonical HRF (and possibly its temporal derivatives) may be sufficient. Indeed, even if the between-region hemodynamics variability is acknowledged, the canonical HRF can provide good results in regions where it has precisely been calibrated such as temporal and occipital cortices as studied by **Boynton et al.** (1996). However, if one is interested in detecting activation in regions involving more complex processes or where potential hemodynamics delays happen due to varying reaction delays or pathological cases, hemodynamic fluctuations influencing detection activation may occur that are not caught by the HRF derivatives or function bases. Moreover, if one is interested in studying the dynamics features of the response, an *explicit* HRF estimation is required. The main question in this case concerns the need for condition-specific features or not, namely for an HRF estimation associated with each experimental condition or for a single HRF estimate associated with all conditions, as proposed in the JDE framework. If explicit condition-wise HRFs are required, the best methodological tool to use is the temporally Regularized FIR (RFIR) developed in **Marrelec et al.** (2003); **Ciuciu et al.** (2003). Otherwise, if variability is expected only across separated and specialized regions, the JDE framework is well-suited. Indeed, within a specialized region, if only one condition exhibits activity then the region-specific HRF can be considered a condition-specific HRF. The performance of RFIR models depends nonetheless on the number of experimental conditions involved in the paradigm because the higher this number, the larger the number of parameters to estimate and thus the fewer the number of degrees of freedom for statistical testing. The model choice depends thus also on the experimental paradigm. First, it is worth noticing that the use of the JDE formulation is less relevant to analyze block paradigm data since the signal

variability in this case is hardly significant. The JDE formalism is actually more adapted to fast event-related paradigms or to paradigms including many conditions, like the localizer paradigm (10 conditions) introduced by **Pinel et al.** (2007) and used hereafter in this paper. The JDE approach is also optimally tuned to combined analysis of hemodynamics features with the detection of activated brain areas. To sum up on the model choice, the JDE model provides a fair compromise with the possibility for the user to adapt the model to the studied region.

With respect to the sole detection aspect, JDE also delivers interesting and complementary results for activation detection compared to classical GLM. It is worth noticing that spatial regularization, which is necessary due to the low SNR in fMRI, is not enforced in the same way between methods. In the GLM, FIR and RFIR cases, there is no embedded spatial regularization within models. Indeed, the data are usually spatially smoothed with a fixed Gaussian kernel as part of preprocessings. In contrast, in the JDE case, spatial correlation is embedded through hidden Markov models. The amount of spatial correlation is automatically tuned and also adaptive across brain regions, therefore avoiding any prior invariant smoothing. As regularization methods require important computational load, a more efficient variational inference scheme have been developed inside the JDE framework in **Chaari et al.** (2013). Of course, the computational cost is less and less a limiting factor with the increase of CPU power and the advent of clusters, parallel processing units and GPGPU. The JDE approach, available in `pyhrf`, has been thought of to be used in daily routine applications with parallel computing resources.

`pyhrf` is mainly written in python with some C code to cope with computationally demanding parts of algorithms. Originally, seminal versions of the implemented methodological tools were available in the matlab HRF toolbox for SPM2. The choice to move to python has been motivated by its free access and its growing dynamical scientific community mainly carried by the `scipy` project. Moreover, compared with matlab, python provides easier prototyping features when it comes to building user interfaces (command lines, GUIs) or linking code from other languages. Finally, this python choice has been made possible thanks to the `nipy` project and especially `nibabel` to handle data reading/writing in the NIFTI format.

In terms of package maturity, `pyhrf` is a research tool which receives various methodological advances relative to fMRI data analysis. However, `pyhrf` has the ambition to target cognitive neuroscientists and clinicians so that efforts are made in terms of user-friendliness. Hence, the design is a trade-off between *mutability* which is required by methodological research where specifications change frequently and *usability* where user interfaces should be as stable as possible to ease external non-developer use cases.

The rest of the paper is organized as follows. First, methods available in the package are presented, comprising parcellation and detection/estimation analyses. Then, the workflow and design of the `pyhrf` package are detailed which cover the user interface and code snippets for the main analysis treatments, simulation framework, distributed computations and data viewer. Results illustrate the outcome of geometrical and functional parcellation and their impact on detection/estimation treatments. Finally, conclusions are drawn and perspective concerning future developments are foreseen.

2 METHODS

The main fMRI data analysis methods available in `pyhrf` are of two kinds: (i) parcellation tools that segment the brain into disjoint sets of positions and (ii) activation detection / HRF estimation tools that highlight correlations between the input experimental paradigm and variations in the measured fMRI signal. The first kind comprises two spatial parcellation tools: Voronoi-based random parcellation, as reviewed by **Aurenhammer and Klein** (2000) and balanced partitioning, developed in **Elor and Bruckstein** (2009). The second kind comprises the GLM introduced in **Friston** (1998), the FIR model described in **Henson et al.** (2000), the RFIR model developed in **Marrelec et al.** (2003); **Ciuciu et al.** (2003) and the JDE approach presented in **Vincent et al.** (2010); **Risser et al.** (2011). The GLM and FIR procedures are provided by `nipy` while RFIR and JDE are originally implemented in `pyhrf`. For

all these methods, we refer to their respective bibliographical references for an extensive presentation of their methodology. Nonetheless, the main aspects of these methods are summarized in what follows with the concern of allowing the comparison between them, especially in terms of model structure and assumptions.

After some details about notation and conventions, we first introduce detection/estimation methods, namely GLM, FIR and RFIR, which require the measured fMRI signal as input and the timing of the experimental paradigm. After setting the generative model common to all detection/estimation methods and a brief comparative overview, each approach is presented in more details. Subsequently, parcellation methods are presented. Spatial parcellation approaches can be applied directly to the input fMRI data and only depend on its geometry. Functional parcellation, which is a clustering of GLM results, is detailed afterwards.

2.1 NOTATION

Conventions We denote vectors with bold lower case (e.g., $\boldsymbol{y}$) and matrices with bold upper case letters (e.g., $\boldsymbol{P}$). A vector is by convention a column vector. Scalars are denoted with non-bold lower case letters (e.g., a). The transpose operation is denoted by ^{t}. Probability distribution functions (pdf) are denoted using calligraphic letters (eg, $\mathcal{N}$ and $\mathcal{G}$ for the Gaussian and gamma distributions). Sequence of integers are denoted as $j = 1 : J$ to indicate a range between 1 and J.

Data geometry As methods can be applied to data defined in the volume or on the cortical surface, the generic term "position" will be used in place of "voxel" (volume unit) or "node" (surface mesh unit). Position indexes are denoted j ($j = 1 : J$). Data are assumed to be masked to only keep positions within the brain. J is the total number of positions within the functional mask. In addition, when considering parcellated data, this functional mask is divided into a set of Γ parcels denoted $\mathbb{P} = \{\mathcal{P}_1, ..., \mathcal{P}_\gamma, ..., \mathcal{P}_\Gamma\}$, $\mathcal{P}_\gamma$ is the set of position indexes belonging to parcel γ. Let us denote $J_\gamma = |\mathcal{P}_\gamma|$ the number of positions in parcel γ.

Functional data We consider the usual case of evoked fMRI data analysis where the experimental paradigm comprising M conditions is known. The signal measured at each time of repetition (TR) is denoted $\boldsymbol{y}_j = \{y_{j,n}\}_{n=1:N}$ where N is the number of scans. Stimulus timing onsets for a given experimental condition $m = 1 : M$ are encoded by variable $\boldsymbol{x}^m$ so that $x_t^m = 1$ if a stimulus occurs at time t up to a time step Δt, else $x_t^m = 0$. The time step is such that $\Delta t \leqslant TR$ and depends on the actual temporal resolution sought by the analysis method.

2.2 DETECTION/ESTIMATION METHODS

For ease of comparison, the presentation of all methods is immersed in the same formalism where the signal is assumed generated by a linear and time-invariant (convolution) system with additive noise. We also consider the usual case of taking into account a position-specific low frequency drift in the data which is a well known fMRI artifact produced by the aliasing of respiratory and cardiac rhythms into the low frequencies as studied in **Yan et al.** (2009). The generic forward model, reads:

$$\boldsymbol{y}_j = \sum_{m=1}^{M} \boldsymbol{X}^m \boldsymbol{\phi}_h^m + \boldsymbol{P}\boldsymbol{\ell}_j + \boldsymbol{b}_j, \tag{1}$$

where:

- $\boldsymbol{P}$ is a fixed orthonormal basis that takes a potential drift and any other nuisance effect (e.g., motion parameters) into account. The low-frequency drift can classically be either polynomial with an order up to 5 or cosine with a cut-off of 0.01Hz,

- $\boldsymbol{\ell}_j$ are the unknown regression weights associated to $\boldsymbol{P}$,
- $\boldsymbol{b}_j$ is the noise component,
- $\boldsymbol{\phi}_h^m$ is a "generic" hemodynamic filter of size D whose definition varies across methods. In the GLM framework, $\boldsymbol{\phi}_h^m$ can be fixed to the canonical HRF or parametric when resorting to function bases and we will note R the number of unknown parameters. In non-parametric approaches, all HRF coefficients are estimated as in RFIR or JDE approaches,
- $\boldsymbol{X}^m$ is the $N \times D$ stimulus occurrence matrix consisting of the lagged stimulus covariates for the experimental condition m: $\boldsymbol{X}^m = \left[\boldsymbol{x}_{t_1}^m, \ldots, \boldsymbol{x}_{t_N}^m\right]^{\mathrm{t}}$ with $\boldsymbol{x}_{t_n}^m = \left(x_{t_n - d\Delta t}^m\right)_{0 \leqslant d \leqslant D}^{\mathrm{t}}$,
- $\sum_{m=1}^{M} \boldsymbol{X}^m \boldsymbol{\phi}_h^m$ is hence the summation of all stimulus-induced signal components which are generated as the convolution between the paradigm encoded in $\boldsymbol{X}^m$ and the hemodynamic filters $\boldsymbol{\phi}_h^m$.

For the sake of simplicity, multiple-run data are not considered here but all implemented methods can handle such data with a fixed-effect model (same effect size across runs), a homoscedastic noise model (one noise variance for all runs) and run-specific drift coefficients.

To give a first overview of how this generative model structure is derived in the different approaches, Table 1 provides a comparison in terms of regularization, number of unknowns and analysis duration. Embedded spatial regularization is only available in the JDE procedure, while temporal regularization is available in RFIR and JDE (Table 1 – 1st, 2nd rows). In terms of constraint applied to the HRF shape (Table 1 – 3rd row), the basis set GLM (BS GLM) is the most constraining and the shape captured depends on the choice of the function basis. In the FIR, RFIR and JDE cases, any form of HRF shape can be recovered, provided that they are smooth in the case of RFIR and JDE. On Table 1 – 4th row, the information on the number of unknowns conveys the level of parsimony of a given model. BS GLM, FIR and RFIR have increasing model complexity as the number of parameters for the HRF increases. In contrast, JDE achieves larger parsimony by making the number of unknowns associated with the HRF dependent on the number of parcels rather than on the number of positions. When computing the ratio between the number of unknowns and the number of data points for a typical fMRI experiment (Table 1 – 5th row), it appears that JDE is comparable to a GLM with derivatives. The RFIR presents the worst situation with 3 times more unknowns than data points. In terms of analysis duration (Table 1 – last row), GLM methods are almost instantaneous as their inference is straightforward. RFIR relies on an iterative scheme to perform unsupervised estimation of the amount of temporal regularization and is hence much slower. In addition, the implementation of RFIR is done in pure python with a main loop over positions which worsen its slow computation speed ($\sim$ 30h. for a whole brain analysis)[1]. Therefore, this approach is rather limited to the processing of some regions of interest where we expect cerebral activity instead of whole brain data analysis. The computation speed of JDE is also slow, but to a lesser extent as results can be obtained overnight ($\sim$ 8h. for a whole brain analysis) on a single processing unit. All these considerations on speed have to be nuanced with the access to increasing computing power and distributed computations, as will be seen in section 3.3.

2.2.1 basis set General Linear Model

In any position j of the brain, the basis set GLM allows (BS GLM) for some limited hemodynamic fluctuations by modeling the hemodynamic filter function $\boldsymbol{\phi}_h$ in Eq. (1) as a weighted sum of the fixed canonical HRF denoted $\boldsymbol{h}_{\mathrm{c}}$ and its first and second order derivative $\boldsymbol{h}_c'$, $\boldsymbol{h}_c''$ as proposed in **Friston** (1998).

[1] Note that the RFIR approach with supervised regularization is much faster with an analysis duration of 20 min. since the maximum a posteriori estimator admits a closed form expression.

Table 1. Comparative overview for all detection/estimation analysis procedures available in `pyhrf` in terms of model structure and analysis duration. "2nd order deriv." stands for a penalization on the energy of the HRF which penalizes abrupt shape changes. The number of nuisance parameters was considered the same for all models, so that only the modeling of the stimulus-induced component is relevant to assess model parsimony. The ratio "unknowns / data" is given for a typical fMRI data analysis with $J = 4 \times 10^4$, $R = 3$, $D = 40$, $M = 10$, $\Gamma = 400$ and $N = 128$ (total number of data points: $N \times J$). The analysis duration is for a whole brain data treatment on an Intel Core i5 (M480 2.67Ghz).

	BS GLM	FIR GLM	RFIR	JDE
Spatial regularization	smoothing	smoothing	smoothing	adaptive
Temporal regularization	none	none	2nd order deriv.	2nd order deriv.
HRF shape constraint	function basis	free	smooth	smooth
Number of unknowns for the stimulus-induced component	$J{\times}R{\times}M$ $1 \leqslant R \leqslant 3$	$J{\times}D{\times}M$ $D \approx 10$	$J{\times}M{\times}(D{+}1)$ $10 \leqslant D \leqslant 50$	$2{\times}J{\times}M + \Gamma{\times}(D{+}4M{+}1)$ $10 \leqslant D \leqslant 50$, $\Gamma \approx 400$
Typical ratio of unknowns / data	0.23	0.78	3.4	0.16
Analysis duration	3 min.	5 min.	30 h.	8 h.

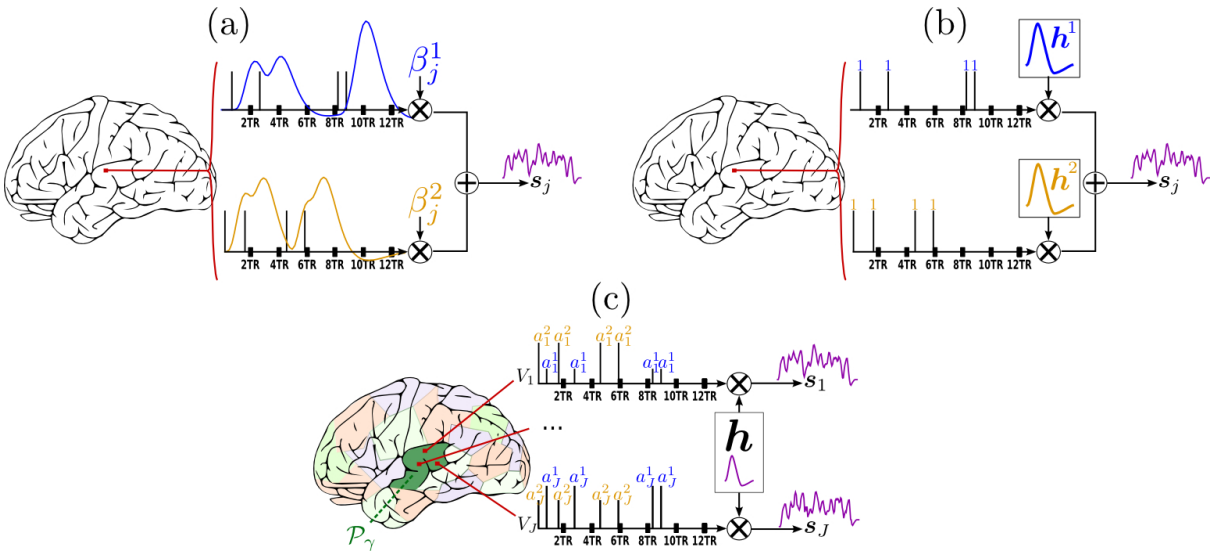

Figure 1. Forward models generating the stimulus-induced components for the methods available in `pyhrf`. In all cases, the scheme involves two experimental conditions colored in blue and yellow with four stimulation events as depicted by vertical bars over the TR-sampled grid. **(a)**: General Linear Model (GLM). For a given condition in a given voxel, the stimulus event sequence is convolved with the fixed canonical HRF resulting in a fixed stimulus-induced regressor. This regressor is then multiplied by an unknown effect β_j^m. All the condition-specific regressors are then summed to form the final stimulus-induced signal s_j. **(b)**: Finite Impulse Response (FIR) Model. In a given voxel, the stimulus event-sequence is convolved with an unknown FIR vector $\boldsymbol{h}^m$ for each condition to yield a condition-specific component. All components are then summed to form the final stimulus-induced signal s_j. **(c:)** Joint Detection-Estimation (JDE). For a given voxel in a given parcel $\mathcal{P}_\gamma$, the stimulus sequence gathering all experimental conditions is multiplied by the response levels $\{a_j^m\}$. Then, this spike signal is convolved with an unknown spatially-invariant HRF $\boldsymbol{h}$ to form the stimulus-induced signal s_j.

The generative model, illustrated in Fig. 1(a), reads:

$$\forall j, \quad \boldsymbol{y}_j = \sum_{m=1}^{M} \boldsymbol{X}^m \left(\beta_j^m \boldsymbol{h}_\mathrm{c} + \beta'^m_j \boldsymbol{h}'_\mathrm{c} + \beta''^m_j \boldsymbol{h}''_\mathrm{c}\right) + \boldsymbol{P}\boldsymbol{\ell}_j + \boldsymbol{b}_j, \tag{2}$$

where β_j^m, β'^m_j, β''^m_j are the unknown effects associated with the mth stimulus-induced regressors constructed with the fixed known vectors $\boldsymbol{h}_c$, $\boldsymbol{h}'_c$, $\boldsymbol{h}''_c$ respectively. Here, the size of $\boldsymbol{h}_c$ is such as

$D = 25/\text{TR}$ for a duration of 25 sec. To obtain the classical GLM with only the canonical HRF, β'_j and β''_j can be set to zero for all positions. It is worth noting that this formulation of the forward model is equivalent to the classical one where all regressors are gathered in the design matrix (noted $\bar{\boldsymbol{X}}$) and all corresponding effects gathered in a single vector $\bar{\boldsymbol{\beta}}$. Eq. (2) can be written as:

$$\forall j, \quad \boldsymbol{y}_j = \bar{\boldsymbol{X}}\bar{\boldsymbol{\beta}}_j + \boldsymbol{b}_j, \tag{3}$$

with:

$$\bar{\boldsymbol{X}} = \left[\boldsymbol{X}^1\boldsymbol{h}_c \,|\, \cdots \,|\, \boldsymbol{X}^m\boldsymbol{h}_c \,|\, \boldsymbol{X}^1\boldsymbol{h}'_c \,|\, \cdots \,|\, \boldsymbol{X}^m\boldsymbol{h}'_c \,|\, \boldsymbol{X}^1\boldsymbol{h}''_c \,|\, \cdots \,|\, \boldsymbol{X}^m\boldsymbol{h}''_c \,|\, \boldsymbol{P}\right]^T,$$

$$\bar{\boldsymbol{\beta}}_j = \left[\beta^1_j \,|\, \cdots \,|\, \beta^m_j \,|\, {\beta'}^1_j \,|\, \cdots \,|\, {\beta'}^m_j \,|\, {\beta''}^1_j \,|\, \cdots \,|\, {\beta''}^m_j \,|\, \boldsymbol{\ell}_j\right]^T.$$

The hemodynamics fluctuations caught by such model are limited to $\sim$1 second around the peak of the canonical HRF which is at 5 sec, see **Calhoun et al.** (2004). This model is massively univariate since every position j is analyzed independently, i.e., no correlation between neighboring signals is considered. Such model works well on spatially smoothed data to counter-balanced the low signal-to-noise ratio, at the expense of blurred activation clusters. In the `nipy` implementation of the GLM, the fitting process can be performed using ordinary least square in the case of white Gaussian noise or using Kalman filtering in the case of an $AR(1)$ Gaussian noise process.

2.2.2 FIR GLM and Regularized FIR

The generative BOLD signal modeling in the FIR context encodes all HRF coefficients as unknown variables:

$$\forall j, \qquad \boldsymbol{y}_j = \sum_{m=1}^{M} \boldsymbol{X}^m\boldsymbol{h}^m_j + \boldsymbol{P}\boldsymbol{\ell}_j + \boldsymbol{b}_j \tag{4}$$

Here, vector $\boldsymbol{h}^m_j = \left(h^m_{j,d\Delta t}\right)^{\mathrm{t}}_{d=0,..,D}$ represents the unknown HRF time course in voxel j which is associated with the mth experimental condition and sampled every Δt. For the FIR GLM, the size of $\boldsymbol{h}$ is such as $D = 25/\text{TR}$ for a duration of 25 sec. Over-sampling could be performed here but is not advisable in terms of estimability since some FIR coefficients may be poorly or even not associated with paradigm covariates in matrix $\boldsymbol{X}^m$, depending on the paradigm jittering. In its un-regularized version, the FIR model can be expressed in the GLM framework and hence its implementation in `pyhrf` relies on `nipy`.

In the case of the Regularized FIR (**Ciuciu et al.** (2003)), the problem is placed in the Bayesian formalism in order to inject regularity on the recovered HRF coefficients $\boldsymbol{h}_j$. More specifically, $\boldsymbol{h}^m_j \sim \mathcal{N}(\boldsymbol{0}, v_{\boldsymbol{h}^m_j}\boldsymbol{R})$ with $\boldsymbol{R} = (\boldsymbol{D}_2^{\mathrm{t}}\boldsymbol{D}_2)^{-1}$ where $\boldsymbol{D}_2$ is the second-order finite difference matrix enforcing local smoothness by penalizing abrupt changes quadratically and $v_{\boldsymbol{h}^m_j}$ is the unknown HRF prior variance which is jointly estimated. The size of $\boldsymbol{h}$ is typically $D = 25/(\text{TR}/4)$ for a duration of 25 sec. and an over-sampling factor of 4. The fitting processed is performed by an Expectation-Maximization (EM) algorithm to evaluate maximum a posteriori (MAP) voxelwise HRF estimators. For computational and inference details about this model, see **Ciuciu et al.** (2003).

2.2.3 Joint Detection-Estimation

The functional mask of a given subject's brain is a priori divided in Γ functionally homogeneous *parcels* using methods described in subsection 2.3.2. In each parcel $\mathcal{P}\gamma$, the shape of the HRF $\boldsymbol{h}_\gamma$ is assumed

constant and the parcel-specific generative model reads:

$$\forall\, j \in \mathcal{P}_\gamma, \quad \boldsymbol{y}_j = \sum_{m=1}^{M} a_j^m \boldsymbol{X}^m \boldsymbol{h}_\gamma + \boldsymbol{P}\boldsymbol{\ell}_j + \boldsymbol{b}_j. \tag{5}$$

where $\boldsymbol{y}_j$, $\boldsymbol{X}^m$, $\boldsymbol{P}$, $\boldsymbol{\ell}_j$ and $\boldsymbol{b}_j$ match the variables introduced in subsection 2.2.1. As for RFIR, the size of $\boldsymbol{h}$ is typically $D = 25/(\mathrm{TR}/4)$ for a duration of 25 sec. and an over-sampling factor of 4. Here a_j^m stands for the Neural Response Level (NRL) in voxel j for condition m. As shown in Fig. 1(c) which illustrates this forward model, the variable a_j^m encodes fluctuations that occur *before* the application of the hemodynamic filter. Therefore, they are assimilated to neural effects, hence termed "Neural Response Levels". However, this term, which is historical, might be misleading as it is difficult to disentangle the contribution of the neural and the vascular components from single BOLD fMRI data. These terms can be more simply identified to the voxel- and condition-specific response amplitudes.

In contrast to Eq. (2) for the GLM forward model, the fixed HRF components $\boldsymbol{h}_c$ and $\boldsymbol{h}'_c$ are replaced by an *unknown* parcel-based HRF $\boldsymbol{h}_\gamma$. Similarly, each unknown NRL a_j^m embodies a single magnitude parameter per regressor whereas the GLM formulation implies that the magnitude is distributed between weights β_j^m, β'^m_j and β''^m_j. To summarize, the HRF shape and the BOLD response magnitude are coupled in the GLM formulation whereas they are decoupled in the JDE formulation.

In the Bayesian framework, priors are formulated to (i) enforce temporal smoothness on the HRF shape to perform estimation in the same manner as for RFIR and (ii) account for spatial correlations between NRLs through spatial mixture models to perform detection, as described in **Vincent et al.** (2010). The regularization factor that controls the amount of spatial regularization is jointly estimated and optimized wrt parcel topology so as to perform an adaptive spatial smoothing. If we are not interested in the estimation of the HRF and the canonical version seems a reliable choice to the experimenter, then the HRF can be fixed to its canonical version in the JDE framework which hence amounts to a *spatially adaptive GLM*. The latter approach enables parcelwise multivariate detection of activations with adaptive regularization across parcels. As shown in **Badillo et al.** (2013b), at the group-level, this strategy retrieves more peaked and less extended activation clusters compared to classical SPM-like analysis.

The inference is performed by a stochastic sampling scheme where posterior mean estimates (or MMSE) are computed from Markov Chain Monte Carlo samples. The implementation of the main sampling loop is coded in pure python and some intensive samplers such as the one for the HRF of the NRLs are coded in C to save computation time. Still, the overall JDE procedure is computationally intensive and a whole brain analysis takes around 10 hours on a single CPU ($N = 128$, $\Gamma = 400$, $M = 10$). However, since there are as many *independent* models as parcels, the analysis can be split up into parcel-wise *parallel* analyses. For specific details about parallel computing, see section 3.3. From a methodological point of view, note that the efficiency of the inference scheme has been improved by resorting to a variational formulation of the JDE **Chaari et al.** (2013) which is also available in `pyhrf`.

2.3 PARCELLATION

2.3.1 Spatial parcellation

Random Voronoi diagrams A Voronoi diagram consists of a spatial partitioning that builds parcels around predefined control points or seeds. The parcel boundaries are placed so that each point of a given parcel is closer to the associated parcel seed than any other seed in terms of the Euclidean distance, as illustrated in Fig. 2(left). Here, the seed positions are randomly chosen and, in the case of a volume data analysis, these positions are limited to a shrunk functional mask so that no seed is placed at the edge of the brain, avoiding peripheral parcels that would be too flat. To build a parcellation from such partitioning, i.e., to assign each cerebral position to a parcel identifier, we do not explicitly require the parcel boundaries. Accordingly,

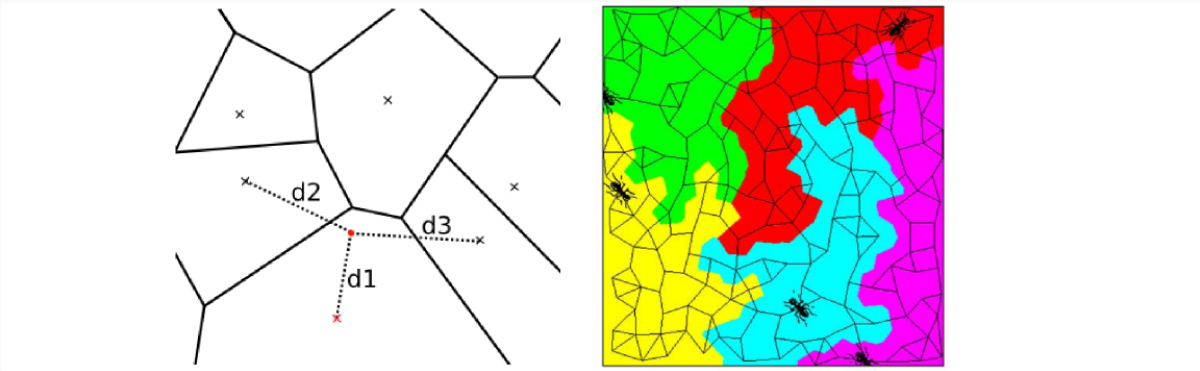

Figure 2. Illustration of spatial parcellation methods in `pyhrf`. **Left:** Voronoi diagram where seeds are represented as crosses. The red point is assigned to the red seed and verifies that its distance to any other seed is larger (d1 $<$ d2, d1 $<$ d3). **Right:** balanced partitioning performed by patrolling a(ge)nts, image extracted from **Elor and Bruckstein** (2009).

there is no need to rely on classical algorithms that precisely compute these boundaries. Instead, a given position is assigned to the id of the closest seed by resorting to a kd-tree ([2]).

Random Voronoi parcellations are convenient ways to generate samples in the space of sensible parcellations as they produce convex and compact parcels which are physiologically plausible. They have been used in **Vincent et al.** (2008) to study the sensitivity of the parcel-based Joint Detection-Estimation method.

Balanced partitioning The goal of balanced partitioning is to build parcels of equal sizes. In the case of a non-regular topology such as the brain, there is no morphological tool to deterministically solve such a partitioning problem which is known to be NP-complete as mentioned in **Andreev and Räcke** (2004). Hence, the algorithm implemented in `pyhrf` employs an heuristic and relies on a multi-agent system that mimics the inflation of balloons in a fixed volume (**Elor and Bruckstein** (2009)), as illustrated in Fig. 2(right).

Balanced partitioning is useful to test the effect of parcel size. In `pyhrf`, balanced partitioning is implemented in pure python with a position-wise main loop and is hence rather slow: ~ 1 minute to split 6000 voxels into 20 parcels. However, this performance is sufficient since we only employ balanced partitioning in the case of small scale testing data sets or when parcels obtained on real data are too big and they would slow down the overall computation too much, especially in the case of distributed computing.

2.3.2 Functional parcellation

The main goal of functional parcellation is to provide homogeneous parcels with respect to hemodynamics. It is mainly motivated by the JDE procedure which assumes that the HRF shape is constant within one parcel, allowing spatial aggregation within the forward modeling. To provide such parcellation, results obtained from a GLM analysis, or any given task-specific functional maps are clustered using different available algorithms: K-means, Ward or spatially-constrained Ward as provided by `scikit-learn`[3]. To objectively choose an adequate number of parcels, theoretical information criteria have been investigated in **Thyreau et al.** (2006): converging evidence for $\Gamma \approx 400$ at a spatial resolution of $3 \times 3 \times 3\,\mathrm{mm}^3$ has been shown for a whole brain analysis leading to typical parcel sizes around a few hundreds voxels ($\approx 2.7\mathrm{cm}^3$). As the parcel size is not fixed, some big parcels may arise from the parcellation process and may slow down the overall parallel processing. To overcome this, the

[2] implemented in `scipy.spatial.KDTree`

[3] `sklearn.cluster.ward`

maximum parcel size was controlled by splitting too big parcels (larger than 1000 voxels) according to the balanced partitioning presented in section 2.3.1, which also guarantees the spatial connexity and thus properly satisfies the JDE assumptions on the HRF.

Such "hard clustering" approach yields sharp parcel boundaries so that smooth transitions between HRF territories cannot be captured. To avoid wrong boundaries, one can resort to over-segmented parcellations (high number of parcels) so that transitions may be better captured.

3 PYHRF

The installation of `pyhrf` relies on the `setuptools` python package and requires the following dependencies: `numpy` and `scipy` for core algorithms, `nibabel` for nifti or gifti input/outputs, `nipy` for the GLM implementation and parcellation tools, `matplotlib` for plots and `PyQT4` for GUIs. Optional dependencies comprise `joblib`, `scikit-learn` and `soma-workflow`. `pyhrf` is mainly intended for linux-based distributions as it has especially been developed under Ubuntu. Installation notes and documentation can be found online at `http://www.pyhrf.org`. Withing the package, the following data files[4] are shipped:

- 2 volumic fMRI data sets (paradigm as CSV files, anatomical and BOLD data files). One serves quick testing while the other is intended for validation/demonstration purpose, which is used to generate results in section 4.3,
- 1 surfacic fMRI data set mainly intended for testing,
- several simulation resources in the form of `png` images to provide 2D maps of various activation labels and HRF territories.

The rest of this section is organized as follows. First, the overall workflow of how to use `pyhrf` is presented, which mainly resorts to command lines and some dedicated GUI tools. Second, to go further into the package architecture and also to address some features available when scripting, the design of `pyhrf` is introduced. Third, distributed computation is explained in terms of resource handling. Finally, the `pyhrf` viewer is presented with a focus on ergonomics.

3.1 WORKFLOW

The typical usage of `pyhrf` relies on shell commands which work on `XML` files. This `XML` format was chosen for its hierarchical organization which suits well the nested nature of the algorithm parametrizations. A dedicated `XML` editor is provided with a `PyQt4` graphical interface for a quicker edition and also a better review of the treatment parameters. When such an `XML` setup file is generated, it defines a default analysis which involves a small volumic real data set shipped with the package. This allows for a quick testing of the algorithms and is also used for demonstration purpose. Here is a typical example of shell commands sequence used to perform a JDE analysis:

```
$ pyhrf_jde_buildcfg -o jde.xml    # generate a default XML file
$ pyhrf_xmledit jde.xml            # set up custom experiment
$ pyhrf_jde_estim -c jde.xml       # run the analysis
$ pyhrf_view *nii                  # view all output nifti files
```

The "buildcfg" command offers various options to define setup items from the command line without having to edit the XML file. For example, the paradigm can be loaded from a CSV or a SPM.mat file. As for the JDE procedure specifically, the option `--vem` enables the variational EM approach developed in **Chaari et al.** (2013).

[4] There is no special licence on the shipped data sets.

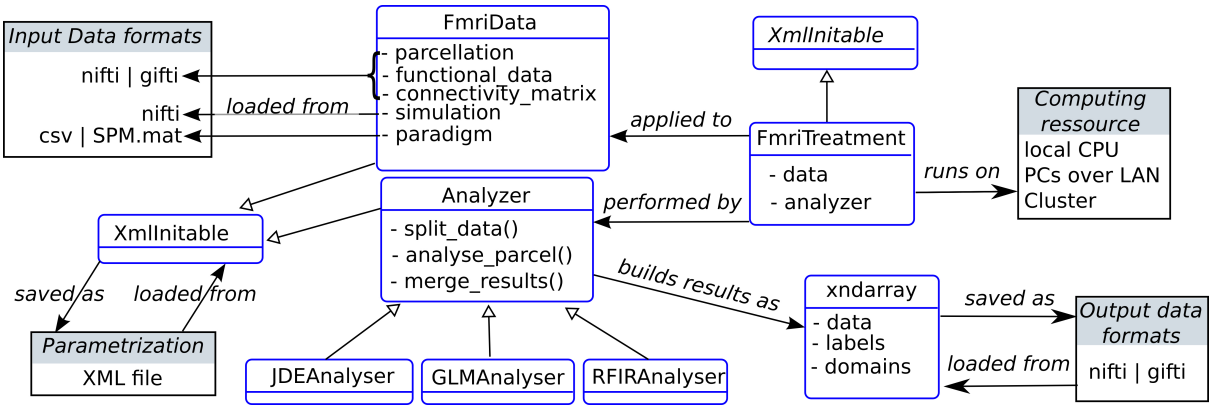

Figure 3. Static organization of the main components in the `pyhrf` package (not exhaustive). Classes are represented as rounded blue rectangles and external resources (file, computing units) as black rectangles. Note that the `XmlInitable` class is duplicated for layout convenience. As in UML class diagrams, arrows have the following meaning: ⟶ stands for an association, ⟶▷ stands for a generalization.

3.2 DESIGN

An overview of the static design of the main package components of the package is shown in Fig. 3. The class `FmriData` is the within-subject fMRI data representation, irrespective of the spatial support: on the cortical surface, in the volume, or from a simulation. The common structure to these various data types comprises spatially flat data (fMRI time series and parcellation) and a connectivity matrix which holds the data topology. At the centre of the analysis component is the `Analyzer` class that handles parcelwise data splitting which is done according to the input data parcellation by default, and also takes care of parcel-specific outputs that are merged at the end of the analysis. This `Analyzer` class is then specialized into various method-specific analyzers: GLM, RFIR and JDE, FIR being just a specific parametrization of the GLM. Note that the analyzer component is decoupled from the data component, as classically done in scientific programming because they do not have the same life-cycles (e.g., the same model can be applied to various data objects). The `FmriTreatment` packs the data and analysis definitions together and handles distributed computation across parcels.

In the following sub-sections, two specific components are further explained: XML parametrization through the `XmlInitable` class, and the handling of arrays with axis semantics through the `xndarray` class.

3.2.1 XML parametrization The XML format was chosen for its hierarchical organization which suits the nested nature of the algorithm parametrizations. Indeed, for a JDE analysis, here is an example of such different levels: `treatment` → `analyzer` → `sampler` → `hrf sampler`. At a given level, different classes may be used as there exist, for example, different `sampler` types depending on the type of prior expressed in the JDE model, so that we require a seamless parametrization process that avoids rewriting code for the building of parameter files each time a new model is tested. To do so, any object whose initialization has to be exposed in the XML configuration file inherits the `XmlInitable` class. This system is not a serialization process as the whole python object is not dumped in the XML. Only the parameters provided to the `__init__` function are stored. In terms of object life cycle, this process handles object creation but is not able to track any subsequent modification. Fig. 4 shows a python code sample that illustrates how the XML file is generated from this nested configuration situation. The resulting `XML` file as viewed by the command `pyhrf_xmledit` is also displayed.

3.2.2 The `xndarray` class: data array with axis semantics The development of semantics-driven operations on data arrays were motivated by the parcel-driven nature of the analysis workflow which

```python
from pyhrf.xmlio import XmlInitable, to_xml
import numpy as np

class FmriTreatment(XmlInitable):
    def __init__(self, input_data=None,
                 analysis_parameters=None):
        XmlInitable.__init__(self)

data = { 'bold_file' : './my_bold.nii',
         'paradigm' : np.array([0,2.3,6.]) }

analysis = { 'model' : 'JDE_MCMC',
             'mcmc_sampling' : {
               'HRF' : { 'duration' : 25,
                         'type' : 'canonical' }}}

treatment_xml = to_xml(FmriTreatment(data, analysis))
f = open('./test.xml','w')
f.write(treatment_xml)
f.close()
```

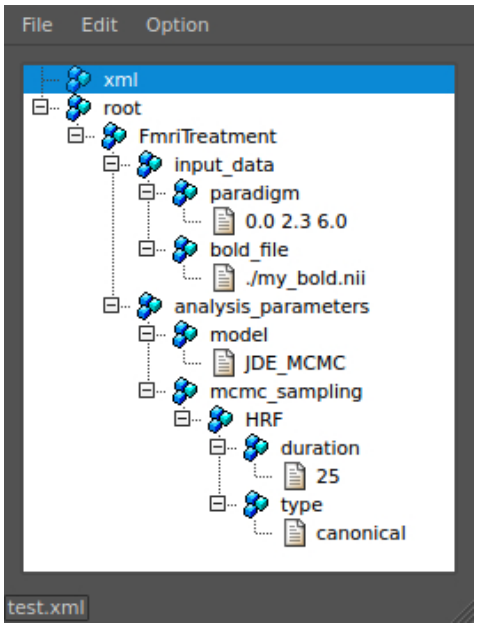

Figure 4. Handling of XML parametrization. The left part shows a code snippet that defines a dummy yet typical fMRI treatment structure with nested components. The init process of the resulting top-level object is then saved in an XML file. The right part is a snapshot of the `pyhrf_xmledit` main window where the XML file generated by the code snippet is browsed.

implied that parcel-specific results have to be merged in a transparent fashion, whatever their shape. Indeed, as `pyhrf` is the repository of all the methodological tools developed within the JDE framework, the number and the form of outputs is highly changing during the development and testing process. This involves producing convergence tracking, intermediate quantities in addition to the final results of interest. To avoid writing specific saving procedure for such versatile and numerous outputs, the information about the interpretation of the data axes has to be explicit. The class `xndarray` handles any required reorientation prior to saving data arrays into nifti or gifti files. In the volumic data case, the reorientation follows the `nibabel` convention that is sagittal, coronal, axial and time. To store the extra axis information along with the data, a dedicated nifti-extension is also written in the volumic data case or add a "pyhrf_xndarray_data" field in the gifti meta data dictionary in the surfacic data case.

Moreover, outputs are primarily generated at the parcel-level so that they are in a flat shape, i.e., the position axis represent indexes of positions in the spatial domain. To form the final whole brain outputs, the parcel-specific outputs have to be merged together and the position axis, if present, has to be mapped into the final spatial domain. Table 2 shows two examples of parcel-specific outputs that are merged to form whole brain data either by spatial mapping or by parcel stacking. To handle these two merging operations, `stack` and `merge` functions are provided. The reverse process is also available via the method `explode` which allows an array to be splitted according to a mask composed of integers, ie a parcellation. It returns the dict of 'flat' parcel-specific data arrays associated with each integer label present in the mask.

In terms of data life cycle, `xndarray` objects are used to prepare data before analysis and to pack results after analysis. During the analysis process, it is more convenient to work with `numpy` arrays directly. The following code snippet illustrates the usage of `xndarray` objects: functional and parcellation data are loaded, within-parcel means are computed and the results is saved to nifti:

```python
from pyhrf.ndarray import xndarray, merge
# Data loading
func_data = xndarray.load('./bold.nii')
```

```
parcellation = xndarray.load('./parcellation.nii')
# Split functional data into parcel-specific data
parcel_fdata = func_data.explode(parcellation)
# Fill parcel-specific data with spatial means
parcel_means = dict( (parcel_id, d.copy().fill(d.mean('position')))
                     for parcel_id,d in parcel_fdata.items() )
# Merge parcel-specific means (map 'position' axis onto spatial axes)
parcel_means = merge(parcel_means, parcellation, axis='position')
# Save output
parcel_means.save('./bold_parcel_means.nii')
```

3.3 DISTRIBUTED COMPUTING

PyHRF provides parallel processing features by exploiting local resources (multiple processors on a single workstation) as well as remote parallel processing units such as a local grid network or a cluster. A whole brain JDE analysis then boils down from 10 hours to 15 minutes in parallel (on a 100-cores cluster). More precisely the available computing resources are handled as follows:

- **local multiple-cores CPUs:** through the use of `joblib` parallel features. The latter works by spawning python sub-processes that are then run on the different processing units by the operating system. The number of used CPUs can be setup by the user.
- **machines over a local area network:** through in-house code that relies on `paramiko` and hence uses *ssh* connections to distribute jobs on the LAN. A basic scheduler is implemented in `pyhrf.grid` that can also report faulty remote runs.
- **multiple-cores cluster:** through `soma-workflow`[5] developed by **Laguitton et al.** (2011), which relies on `paramiko`[6] on the client side and on `DRMAA`[7] on the server side.

[5] http://brainvisa.info/soma-workflow/
[6] http://www.lag.net/paramiko/
[7] http://www.drmaa.org/

Table 2. Examples of merging operations performed on multiple parcel-specific data arrays, for some JDE outputs: parcel-specific HRFs and condition- and voxel-specific activation labels. If the xndarray object contains the "position" axis, as for the "labels" object, then all parcel-specific results are merged into the same target volume and we depict the spatial mapping operation as "→" to map the "position" axis in to the spatial axes "axial", "coronal" and "sagittal". For other axes aside from "position", no merging operation is performed ("=" symbol). If the xndarray object does not contain the "position" axis, as for the HRF object, then all parcel-specific results are stacked and a new "parcel" axis is created ("∪" symbol).

	Parcel-specific flat data		Merging operation	Whole brain data	
	axis label	axis domain		axis label	axis domain
HRF	time	[0, ..., hrf_duration]	=		*same*
			∪	parcel	[0, ..., parcel_max]
labels	class	['activ', 'non_activ']	=		*same*
	condition	['audio, 'video']	=		*same*
	position	[0, ..., pos_max]	→	axial	[0, ..., axial_max]
				coronal	[0, ..., coronal_max]
				sagittal	[0, ..., sagittal_max]

The distribution problem addressed here is a so-called embarrassingly parallel problem where the same treatment has to be repeated on several parcel-specific pieces of data. There is no shared memory management between distributed processes here.

To optimize the distribution process, the order in which the parcel-specific treatments are pushed in the process queue is done by pushing the biggest parcels first. In the same optimization purpose, a safeguard is imposed on the maximum parcel size (more than 7 cm^3 in the volume or 11 cm^2 on the surface). If a parcel exceeds this limit, it is divided up according to the balanced partitioning presented in sub-section 2.3.1.

3.4 VIEWER

`pyhrf_view` is a dedicated viewer built on `PyQt4` which embeds a `matplotlib` view. The purpose of `pyhrf_view` is to provide convenient browsing into volumic data[8]. However, it does not provide advanced overlaying features such as the display of functional over anatomical data. Instead, to plot the final "publication-ready" maps after having selected the results of interest with pyhrf_view, one can resort to the command pyhrf_plot_slice to directly generate a slice image of functional rendering along with anatomical overlay. One can also use a third party viewer such as Anatomist[9], FSL_view[10] or xjview[11].

`pyhrf_view` offers n-dimensional browsing while most viewers in neuro-imaging software handle up to 4D volumes. In fact, there is a limit to the number of dimensions inherent to the nifti format which permits 7 axes at maximum. The viewer is composed of two main components (see 5:

- a main window handling object and slice selection,
- plot windows which display the selected slice as curve or image.

The slice selection tools provides sliders to browse through axes domain values and display related information: axis name, current selected domain values and projection states. There can be up to two projected axes (2D), i.e., axes which will mapped to the actual plot axes. When multiple objects are loaded, slicers are synchronized to plotting views so that click events yield slider updates. This behavior can be modified in two ways. First, the reception combo box toggles whether the slider receives changes from other sliders. This is useful when one wants to prevent a given view from being updated by synchronization events (with reception off), e.g., when a reference slice should be compared to other slices. Second, the emission combo box toggles the spreading of slider changes to all other slicers. This is typically used to control a given axis across all displayed objects with a single slider (with emission on).

4 RESULTS

4.1 EXPERIMENTAL PARADIGM

In all presented results, whether they focus on artificial or real data sets, we resorted to the same experimental paradigm. The latter is a multi-functional cognitive localizer paradigm designed in **Pinel et al.** (2007). This paradigm enables to map cognitive brain functions such as reading, language comprehension and mental calculations as well as primary sensory-motor functions. It consists of a *fast event-related* design (sixty stimuli) comprising the following experimental conditions: auditory and visual sentences, auditory and visual calculations, left/right auditory and visual clicks, horizontal and vertical checkerboards. The average ISI is 3.75 sec. including all experimental conditions. Such a paradigm is well-suited for simultaneous detection and estimation, in contrast to slow event-related and block paradigms which are considered optimal only for estimation or detection, respectively (**Liu et al.** (2001)).

[8] Surface rendering is not available. `Anatomist` is recommended for such usage

[9] `http://brainvisa.info`

[10] `http://fsl.fmrib.ox.ac.uk/fsl/fslview/`

[11] `http://www.alivelearn.net/xjview8/`

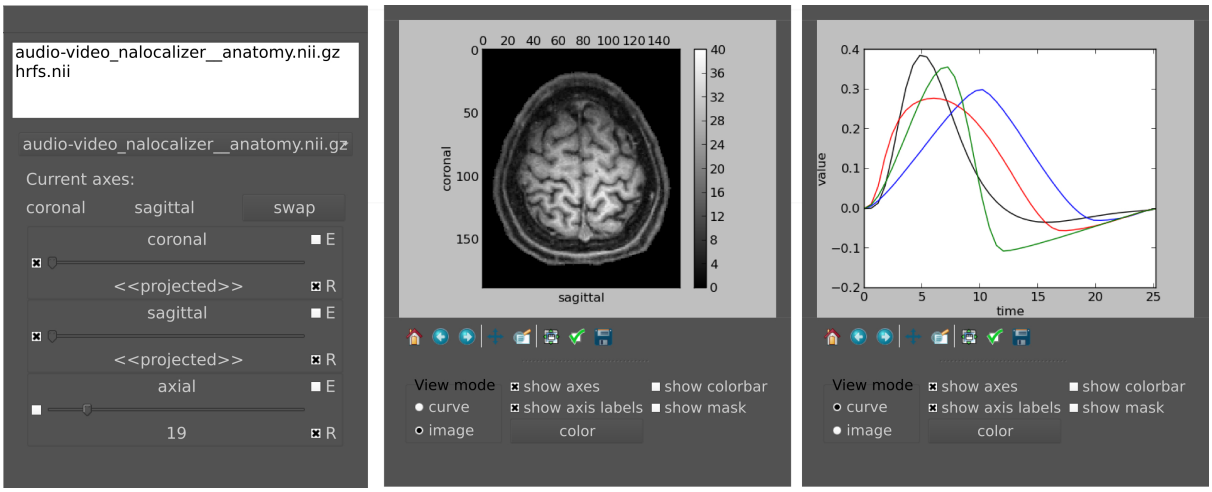

Figure 5. Main widget components of `pyhrf_view` to browse and view n-dimensional data. **Left:** the list widget on top displays the currently loaded objects. The slicer panel at the bottom allows: projection of axes (combo boxes on the left), domain value slicing (sliders in the middle) and definition of view synchronization (combo boxes on the right). For a given axis slicer, the two combo boxes defining synchronization are: (E) toggle emission of slice change to other slicers, (R) toggle reception from other slicers or from click events on plots. **Middle:** plot window for the current selected slice. The top part displays the actual plot as produced by `matplolib.pylab`. The bottom part offers changing the view mode (either curve, image, or histogram), and toggling display of axes, colorbar and mask. The color button pops up a gradient map selector if in image mode or a color picker if in curve mode. **Right:** other plot window to illustrate curve display.

4.2 ARTIFICIAL DATA GENERATOR

Simulations in `pyhrf` mainly consists of building a script that defines a simple pipeline organization. Indeed, the process of generating fMRI data involves many versatile simulation bricks with various dependencies between them as shown in Table 3 which presents the generation processes available in `pyhrf`. Writing a simulation script as a sequence of functions makes things difficult to read and to reuse. Instead, all simulation bricks are gathered inside a python dictionary that maps a simulation label to its corresponding value. This value can be directly defined as a python object or as a function which can depend on other simulation items and which is called when the simulation pipeline is evaluated. The pipeline structure arises from the link between simulation labels and function arguments. In practice, an example of such simulation script is as follows:

```
import numpy as np
from pyhrf.ndarray import xndarray
from pyhrf.tools import Pipeline

# Functions used to generate items in the simulation Pipeline
def generate_rls(spatial_shape, mean_rls, var_rls):
    rls = np.random.randn(*spatial_shape) * var_rls**.5 + mean_rls
    return xndarray(rls, ['axial', 'sagittal', 'coronal'])

def generate_noise(stim_induced_signal, noise_var):
    noise = np.random.randn(*stim_induced_signal.data.shape) * noise_var**.5
    return xndarray.xndarray_like(stim_induced_signal, data=noise)

def create_stim_induced_signal(rastered_paradigm, hrf, response_levels):
    signal = np.convolve(rastered_paradigm, hrf)[np.newaxis,:] * \
                        response_levels.data[:,:,:,np.newaxis]
    return xndarray(signal, response_levels.axes_names + ['time'])
```

```
def create_bold(stim_induced_signal, noise):
    return stim_induced_signal + noise

# Definition of the simulation pipeline
simulation_steps = {
  'spatial_shape' : (10,11,12), 'mean_rls' : 3., 'var_rls' : 0.5,
  'response_levels' : generate_rls,
  'rastered_paradigm' : np.array([0,0,1,0,0,0,1,0,0,0,1]),
  'hrf' : np.array([0,.5,1,0.5,0.,0]),
  'noise_var' : 1.,
  'noise' : generate_noise,
  'stim_induced_signal' : create_stim_induced_signal,
  'bold' : create_bold,
  }

simulation = Pipeline(simulation_steps)

# Computation of all quantities in the pipeline and data saving
simulation.resolve()
simulation_items = simulation.get_values()
simulation_items['response_levels'].save('./response_levels.nii')
simulation_items['stim_induced_signal'].save('./stim_induced_signal.nii')
simulation_items['bold'].save('./bold.nii')
```

The artificial data experiment presented here comprises the generation of BOLD time series within the volume and then projected onto the cortical surface. To do so, shipped data defines a volume of 4 HRF territories, as well as the grey/white matter segmentation obtained from real data in the occipital region. Within the grey matter mask, activation labels are generated and conditionally to them, response levels are simulated according to a bi-Gaussian mixture. For the sake of simplicity, a version of the localizer paradigm presented in the previous section is merged over the auditory and visual modalities so as to obtain only two conditions. In all HRF territories this paradigm is then convolved with HRF generated by Bezier curves that enable the control of the time-to-peak and time-to-undershoot. Finally, nuisance signals are added (Gaussian noise and polynomial drift) to obtain the volume of artificial BOLD data. To generate surfacic data, data are projected on a cortical fold that is also shipped in the package and we resorted to an external projection tool, developed in **Operto et al.** (2006) but others are available such as `Freesurfer`. Fig. 6 presents the results obtained on artificial data using the JDE procedure. HRF estimates recover their respective ground truth profiles with a slightly more deformed curve obtained on the cortical surface for the bottom right (green) HRF territory, compared with the volumic data case. Detection results (response levels maps in Fig. 6) also shows the correct recovery of the simulated ground-truth, in the volume and on the cortical surface.

Table 3. Different types of simulation bricks available in `pyhrf`. The "localizer" paradigm is described in **Pinel et al.** (2007). Hand-drawn maps for activation labels are in the form of `png` images. Gaussian smooth generation of HRFs stands for the regularized prior used in the JDE model.

Simulation item	available generation process
Experimental paradigm	localizer, random event-related
Activation labels	hand-drawn 2D maps, 3D Potts realizations
Response levels	bi / tri mixture of Gaussian or Gamma components
Hemodynamic response function	canonical, Bezier curve, Gaussian smooth
Low frequency drift	polynomial, cosine
Noise	white, auto-regressive of order p

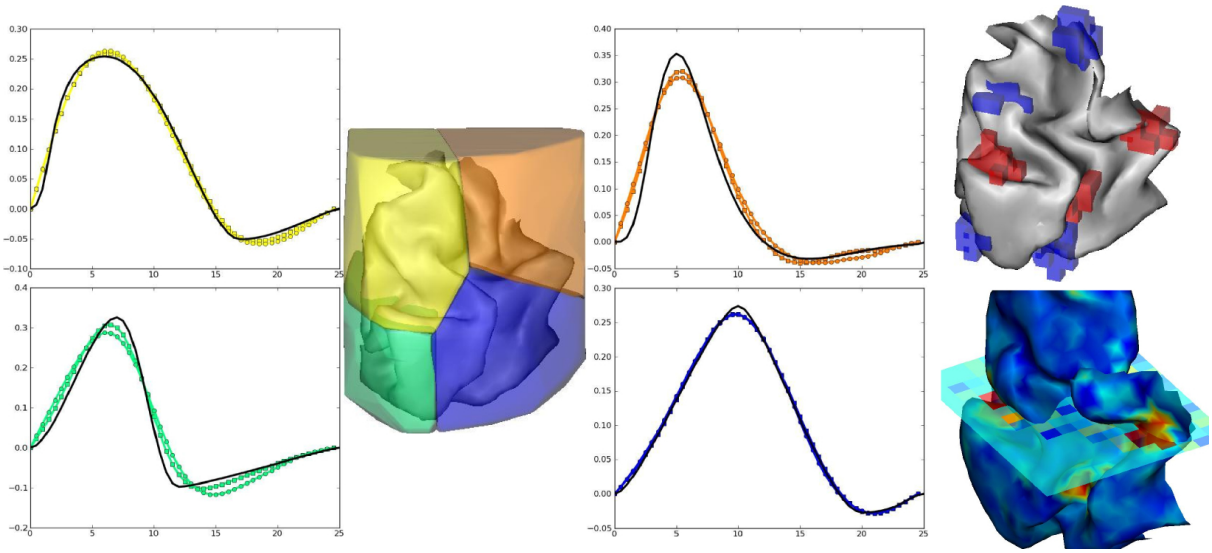

Figure 6. Results on volumic and surfacic artificial data. **Left part**: HRF estimates obtained by JDE on the 4 artificial parcels. Ground truth HRFs are depicted in black line while colored HRF are HRF estimates that match the color of the parcels. Right part, top: labels simulated in the cortical fold for two conditions (in blue and red). **Right part, bottom**: response levels estimates obtained by JDE on the cortical surface and in a selected slice of the volume. 3D renderings were produced with `anatomist`.

4.3 WITHIN-SUBJECT METHOD COMPARISON

The analyzed real data set, which is shipped with `pyhrf`, was a subset of an fMRI acquisition performed on a single healthy subject with a 3-Tesla Tim Trio Siemens scanner using an EPI sequence. The following settings were used for this acquisition: the fMRI session consisted of $N = 128$ scans, each of them being acquired using TR $= 2400$ ms, TE $= 30$ ms, slice thickness: 3 mm, transversal orientation, FOV $= 192$ mm^2 and spatial in-plane resolution was set to 2×2 mm^2. Data was collected using a 32 channel head coil to enable parallel imaging during the EPI (R=2) acquisition. Parallel SENSE imaging was used to keep a reasonable Time of Repetition (TR) value in the context of high spatial resolution. In order to reduce disk usage and to focus only on areas of the brain which are expected to elicit activity in response to the paradigm, functional data was restricted to selected regions of interest that comprise occipital, temporal, parietal and motor regions. To improve interpretation and data plot rendering, an anatomical image is also shipped, with an in-plane resolution of 1×1 mm^2 and slice thickness of 1.1 mm.

This fMRI data set was analyzed using GLM with a canonical HRF, FIR, RFIR and JDE[12]. For JDE, the functional parcellation was built according to the method described in section 2.3.2. Fig. 7(a-b) depicts detection results for the auditory effect, obtained by GLM with canonical HRF (see Fig. 7(a)) and JDE (see Fig. 7(b)). Both methods highlight the same activation localization, with a slightly stronger sensitivity for JDE. Fig. 7(c) shows HRF estimation results as obtained by FIR, RFIR and JDE at the same local maximum on the left temporal region. Note that the HRF estimate provided by the JDE procedure is regional. The HRF profile delivered by FIR appears noisier than the JDE and RFIR counterparts. Also the temporal resolution of FIR is limited to the TR of input data. In contrast, RFIR and JDE offer an enhanced temporal resolution of 0.6 sec. In terms of timing, the FIR and JDE methods yield a peak at 5 seconds which is compatible with the canonical HRF that has been fitted on temporal auditory regions (**Boynton et al.** (1996)). Accordingly, the HRF estimates obtained by RFIR seems over-smoothed. Overall, JDE enables reliable activation maps *and* HRF profiles which can roughly be obtained by separate GLM and FIR analyses. Fig. 7(d-e) shows results on effect maps for the computation effect, obtained by GLM with canonical HRF (see Fig. 7(d)) and JDE (see Fig. 7(e)). JDE results have a higher sensitivity which can be

[12] analysis scripts are available at `http://github.com/pyhrf/pyhrf/tree/master/script/frontiersBIM14/`

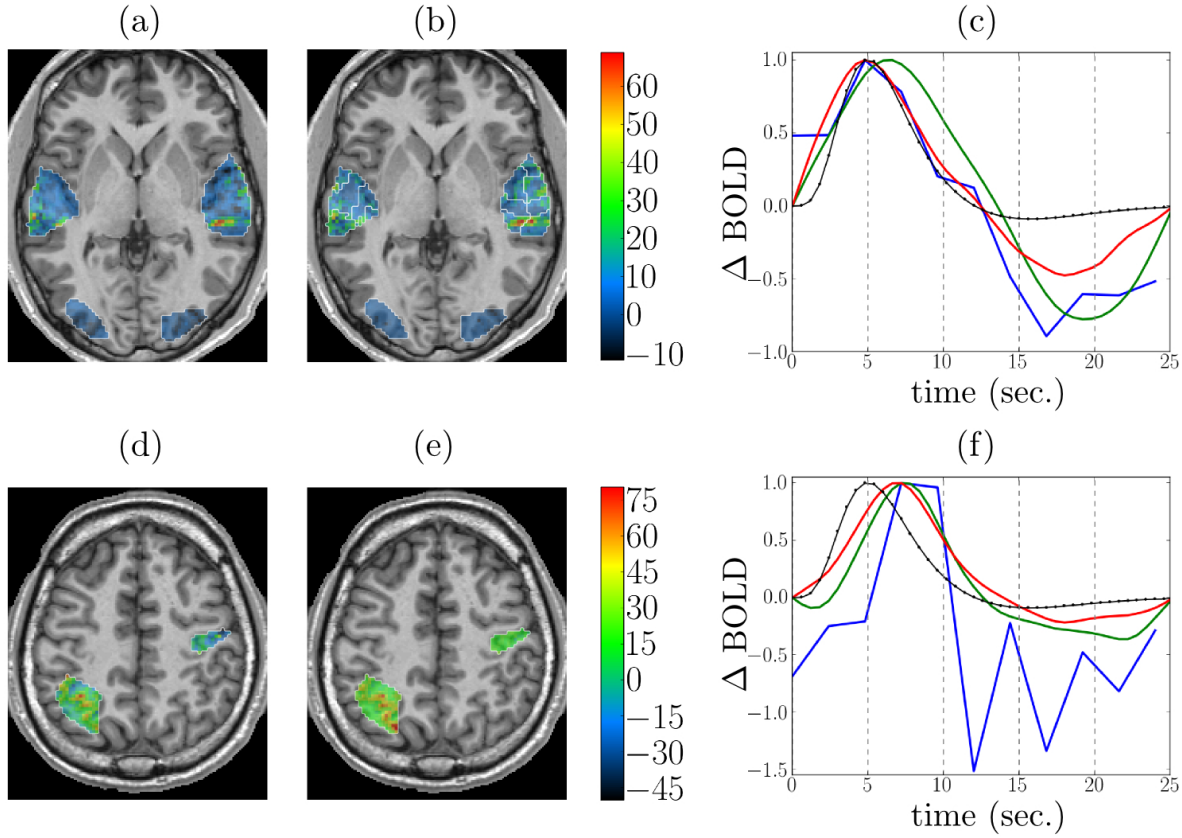

Figure 7. Detection and estimation results on the shipped real data set. Top and bottom rows: auditory and computation experimental conditions, respectively. Columns from left to right: response level maps, for **(a,d)** GLM with canonical HRF, **(b,e)** JDE, superimposed with the functional parcellation (white borders). Neurological convention: left is left. **(c):** Estimation results for GLM FIR (blue), RFIR (green) and JDE (red). The canonical HRF is shown in black.

explained by an estimated HRF that differs from the canonical version (see Fig. 7(f)). More specifically on the HRF estimation results shown in Fig. 7(f), we can draw the same comments as for the auditory results. However, the FIR HRF profile is here more chaotic and its peak is less easy to identify as the curve shows a plateau between 7 and 10 sec.

4.4 GROUP-LEVEL HEMODYNAMICS

Using `pyhrf`, the hemodynamic variability was also studied on a group of 15 healthy volunteers (average: 23.2 years, std: 2 years). The experimental paradigm is described in Section 4.1 and the fMRI acquisition parameters are similar to those previously mentioned in subsection 4.3. The results presented hereafter have been published in **Badillo et al.** (2013b). In this work, hemodynamic variability was investigated in four regions of interest, located in the left parietal cortex (P), bilateral temporal (T) and occipital (O) lobes and in the right motor cortex (M), as shown in Fig. 8. These regions were defined after conducting a random-effect analysis to detect activation clusters showing a significant group-level effect. More precisely, we defined four contrasts of interest targeting brain activity in sensory and cognitive regions: a *Auditory vs. Visual* contrast for which we expect evoked activity in temporal regions in response, a *Visual vs. Auditory* contrast that induces evoked activity in the occipital cortex, a *Left vs. Right click* contrast for which we expect evoked activity in the right contralateral motor cortex, and a *Computation vs. Sentence* contrast which is expected to highlight activity in the frontal and parietal lobes specific to mental calculations. In terms of detection performance, at the group-level, JDE and GLM are comparable in primary sensory regions (where the canonical HRF is appropriate). However, in the parietal region

involved in higher cognitive processes, the JDE approach yields more sensitive maps. In what follows, we summarize group-level hemodynamics results obtained in the regions of interest extracted from activated clusters.

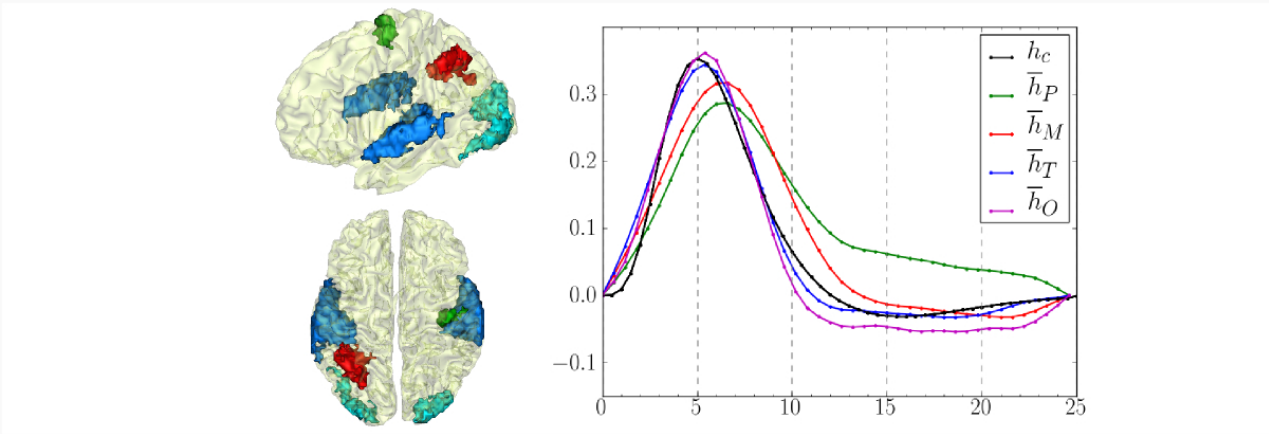

Figure 8. Left: Definition of regions of interest to investigate hemodynamics variability from JDE-based group-level analysis. **Top**: Sagittal view. **Bottom**: axial/top view. Left parietal area (P) appears in red, left motor area in the pre-central cortex is shown in green, Bilateral temporal regions along auditory cortices and bilateral occipital regions in the visual cortices are shown in blue and cyan, respectively. **Right**: Group-average HRF estimates for the four regions of interest: $\bar{\boldsymbol{h}}_P$, $\bar{\boldsymbol{h}}_M$, $\bar{\boldsymbol{h}}_T$, $\bar{\boldsymbol{h}}_O$ stand for HRF means in parietal, motor, temporal and occipital regions, respectively. $\boldsymbol{h}_c$ correspond to the canonical HRF.

The group-level HRF extraction in each ROI involves the following steps: For each subject, we identified the parcel containing the mostly activated voxel across stimulus-dependent response levels. Each individual parcel-based HRF time course is then scaled by the corresponding maximum response level so as to account for the inter-subject variability of the effect size. Last, each group-level HRF profile (see Fig. 8) is computed as the average over the 15 subjects in the corresponding ROI.

One of the main results concerns the spatial gradient of discrepancy to the canonical HRF shape between regions. As shown in Fig.. 8, the mean HRF time courses retrieved in occipital and temporal regions are the closest to the canonical shape $\boldsymbol{h}_c$. In the motor cortex, the HRF deviates a little bit more from the canonical filter, especially in terms of hemodynamic delay. Finally, the largest discrepancy to the canonical HRF was found in the parietal region.

5 PERSPECTIVES

5.1 METHODOLOGICAL PERSPECTIVES

Methods that derive from former external works (GLM, FIR, RFIR), are mainly used for comparison purpose and are not the subject of extension. The main methodological developments are currently taking place in the JDE framework. In fMRI activation protocols, the paradigm usually consists of several runs repeating similar sequences of stimuli. For an increased stability of HRF estimates that cope with the between-run variability of the response magnitude, a multi-run extension has been developed in **Badillo et al.** (2013c), consisting of a random-effect heteroscedastic approach. It is particularly useful for pediatric imaging where runs are short in time. In the same vein of improving within-subject analyses, an approach to encode the condition-specificity at the parcel level is being developed to enforce non-relevant conditions to yield null activation, as in **Bakhous et al.** (2013).

In terms of computation cost, we mentioned the variational EM version of JDE that has been published in **Chaari et al.** (2013) and that appeared to be 10 to 30 times faster than its MCMC alternative. We have also shown that this numerical speed up is not performed at the expense of the result quality in

terms of activation maps and HRF estimates. This algorithmic improvement has allowed us to address a more computationally demanding task, namely the joint Parcellation-Detection-Estimation (JPDE) model **Chaari et al.** (2012) that jointly estimate the spatial aggregation support of HRF shapes, also termed parcellation, whereas the current JDE approach relies on a fixed prior decomposition in homogeneous territories. The JPDE validation is still ongoing. In an attempt to solve the same issue, an alternative based on random parcellations and consensus clustering has been recently proposed in **Badillo et al.** (2013a).

Closely related to the results presented in Section 4.4, a multi-subject extension of the JDE is currently developed to properly account for the between-subject HRF variability and recover a meaningful and potentially less biased group-level HRF profile. Indeed, the group-level results presented so far were computed as a simple mean of multiple within-subject JDE analyses. In presence of outliers, the mean estimator is directly impacted and we thus seek for more robust group-level estimates. This issue can thus be answered either by considering robust group-level averaging techniques (weighted or trimmed least squares, median or Huber M-estimators, ...) or by adding an additional layer in the hierarchical Bayesian modeling. This development trail will bring modification in the core design of `pyhrf` so as to take into account the new "group" data axis.

Finally, recent works have opened the path to multi-modality by the processing of Arterial Spin Labeling fMRI data **Vincent et al.** (2013). To analyze such data, physiologically-inspired models are investigated to establish parsimonious and tractable versions of physiological models such as the balloon model described in **Friston and Buechel** (2000); **Buxton et al.** (2004). Hence, for validation purpose, the artificial data generator is also being enriched with the simulation of physiological models.

5.2 PACKAGE PERSPECTIVES

In addition to improving the documentation and usability of the current package version, additional developments will be first motivated by the above-mentioned methodological perspectives, namely re-factoring part of the data design to integrate the group-level and multi-session data components. This will mainly involve the modification of the `FmriData` class and the addition of a new `FmriGroupData` class. In this respect, the handling of data input will have to be extended to exploit a hierarchy of subject-specific files.

In another respect, we plan on enriching the parcellation component by handling classical atlases such as the Automated Anatomical Labeling (AAL) atlas built by **Tzourio-Mazoyer et al.** (2002), the Brodmann regions (**Brodmann** (1909)) and the Harvard-Oxford atlas (**Desikan et al.** (2006)) available in `FSL` [13]. The goal is to enable the definition of functional parcels that are consistent with previous studies in the literature and also to further investigate the anatomo-functional link by comparing atlas-driven versus data-driven parcellations.

In order to offer more user-friendliness, the building of a unified graphical user interface is foreseen, which will gather the XML editor and the viewer while also enabling the selection of the analysis type. We also envisage resorting to wizard interfaces to guide the setup process and deliver contextual documentation. In terms of browsing features, tools to properly explore the surface-based results are currently missing, as we resort to an external tool, `anatomist`. The goal is not to reproduce all the features offered by the latter which enable the output of paper-ready figures through joint volume/surface rendering, data fusion and material handling. We rather think of a simple textured mesh viewer associated with a picking feature in order to synchronize other views. The main usage is to make the selection of a mesh node and the corresponding HRF estimate feasible. For making this surface-based rendering av available, `mayavi`[14] is an appealing candidate since it has been already intensively used in the python community.

[13] `http://http://fsl.fmrib.ox.ac.uk`

[14] `http://code.enthought.com/projects/mayavi/`

Finally, for the computational efficiency aspect, we plan on incorporating GPU parallel computing features. Indeed, this technology is becoming more and more available and powerful and may also appear cheaper than CPU computing systems (see **Owens et al.** (2008) for a review). Specifically, the NVIDIA chipsets are easily accessible for general purpose computing through the python package `pyCUDA`[15]. A simple test on matrix products with a complexity similar to that of our models showed a gain of one order of magnitude in favor of GPU computations[16] (NVIDIA GeForce 435M graphics card) compared to CPU-based computations (Intel Core M480 @ 2.67GHz) with `numpy`.

6 CONCLUSION

The `pyhrf` package provides tools to detect evoked brain activity and estimate the underlying dynamics from fMRI data in the context of event-related designs. Several "reference" methods are available: the GLM, FIR and RFIR approaches, and also more flexible models as provided by the JDE framework. The choice of the analysis tools depends on the experimenter's question: if simple mappings are required, the GLM is appropriate provided that the HRF is expected to be close to its canonical version, but for finer dynamics estimation, the JDE procedure is more suitable. The design of `pyhrf` allows the handling of volumic and surfacic data formats and also the utilization of several distributed computing resources. The main user interface is done by shell commands where the analysis setup is stored in an XML configuration file. Two graphical components are provided: an XML editor and a n-dimensional volumic data browser.

This package provides valuable insights on the dynamics of the cognitive processes that are not available in classical software such as `SPM` or `FSL`. Hence, it offers interesting perspectives to understand the differences in the neuro-vascular coupling of different populations (infants, children, adults, patients, etc.).

REFERENCES

Andreev, K. and Räcke, H. (2004), Balanced graph partitioning, in Proceedings of the sixteenth annual ACM symposium on Parallelism in algorithms and architectures (ACM, New York, NY, USA), SPAA '04, 120–124

Aurenhammer, F. and Klein, R. (2000), Voronoi Diagrams. (Elsevier Science Publishing), chapter 5, 201–290

Badillo, S., Varoquaux, G., and Ciuciu, P. (2013a), Hemodynamic estimation based on consensus clustering, in IEEE Pattern Recognition in Neuroimaging (PRNI) (Philadelphia, USA)

Badillo, S., Vincent, T., and Ciuciu, P. (2013b), Group-level impacts of within- and between-subject hemodynamic variability in fMRI, *Neuroimage*, 82, 433–448

Badillo, S., Vincent, T., and Ciuciu, P. (2013c), Multi-session extension of the joint-detection framework in fMRI, in 10th International Symposium on Biomedical Imaging (San Francisco, CA), 1504–1507

Bakhous, C., Forbes, F., Vincent, T., Dojat, M., and Ciuciu, P. (2013), Variational variable selection to assess experimental condition relevance in event-related fMRI, in 10th International Symposium on Biomedical Imaging (San Francisco, CA), 1500–1503

Boynton, G. M., Engel, S. A., Glover, G. H., and Heeger, D. J. (1996), Linear systems analysis of functional magnetic resonance imaging in human V1, *The Journal of Neuroscience*, 16, 13, 4207–4221

Brodmann, K. (1909), Vergleichende Lokalisationslehre der Grosshirnrinde (Barth, Leipzig)

Buxton, R. B., g, K. U., Dubowitz, D. J., and Liu, T. T. (2004), Modeling the hemodynamic response to brain activation, *Neuroimage*, 23, Supplement 1, S220–S233

[15] `http://developer.nvidia.com/pycuda`

[16] benchmark available at `http://wiki.tiker.net/PyCuda/examples/DemoMetaMatrixmulCheetah`

Calhoun, V. D., Stevens, M. C., Pearlson, G. D., and Kiehl, K. A. (2004), fMRI analysis with the general linear model: removal of latency-induced amplitude bias by incorporation of hemodynamic derivative terms, *NeuroImage*, 22, 1, 252 – 257

Chaari, L., Forbes, F., Vincent, T., and Ciuciu, P. (2012), Adaptive hemodynamic-informed parcellation of fMRI data in a variational joint detection estimation framework, in 15th Proceedings MICCAI (Springer Verlag, Nice, France), LNCS 7512, (Part III), 180–188

Chaari, L., Vincent, T., Forbes, F., Dojat, M., and Ciuciu, P. (2013), Fast joint detection-estimation of evoked brain activity in event-related fMRI using a variational approach, *IEEE Transactions on Medical Imaging*, 32, 5, 821–837

Ciuciu, P., Poline, J.-B., Marrelec, G., Idier, J., Pallier, C., and Benali, H. (2003), Unsupervised robust non-parametric estimation of the hemodynamic response function for any fMRI experiment, *IEEE Transactions on Medical Imaging*, 22, 10, 1235–1251

Desikan, R. S., Ségonne, F., Fischl, B., Quinn, B. T., Dickerson, B. C., Blacker, D., et al. (2006), An automated labeling system for subdividing the human cerebral cortex on mri scans into gyral based regions of interest., *Neuroimage*, 31, 3, 968–980

Duyn, J. and Koretsky, A. (2011), Novel frontiers in ultra-structural and molecular MRI of the brain, *Curr. Opin. Neurol.*, 24, 4, 386–393

Elor, Y. and Bruckstein, A. M. (2009), Multi-a(ge)nt graph patrolling and partitioning, in Proceedings of the 2009 IEEE/WIC/ACM International Joint Conference on Web Intelligence and Intelligent Agent Technology - Volume 02 (IEEE Computer Society, Washington, DC, USA), WI-IAT '09, 52–57

Friston, K. (1998), Imaging neuroscience: Principles or maps?, *Proceedings of the National Academy of Sciences of the United States of America*, 95, 796–802

Friston, K. and Buechel, C. (2000), Attentional modulation of effective connectivity from V2 to V5/MT in humans, *Proceedings of the National Academy of Sciences of the United States of America*, 97, 13, 7591–7596

Friston, K., Holmes, A. P., Poline, J.-B., Grasby, P., Williams, S., Frackowiak, R., et al. (1995), Analysis of fMRI time-series revisited, *Neuroimage*, 2, 45–53

Henson, R., Andersson, J., and Friston, K. (2000), Multivariate SPM application to basis function characterisations of event-related fMRI responses, volume 11, 468

Koslow, S. H. and Huerta, M. F., eds. (2013), Neuroinformatics: An Overview of the Human Brain Project (Psychology Press)

Laguitton, S., Rivire, D., Vincent, T., Fischer, C., Geffroy, D., Souedet, N., et al. (2011), Soma-workflow: a unified and simple interface to parallel computing resources, in MICCAI Workshop on High Performance and Distributed Computing for Medical Imaging (Toronto)

Liu, T., Frank, L., Wong, E. C., and Buxton, R. B. (2001), Detection power, estimation efficiency, and predictability in event-related fMRI, *Neuroimage*, 13, 4, 759–773

Makni, S., Ciuciu, P., Idier, J., and Poline, J.-B. (2005), Joint detection-estimation of brain activity in functional MRI: a multichannel deconvolution solution, *IEEE Transactions on Signal Processing*, 53, 9, 3488–3502

Makni, S., Idier, J., Vincent, T., Thirion, B., Dehaene-Lambertz, G., and Ciuciu, P. (2008), A fully Bayesian approach to the parcel-based detection-estimation of brain activity in fMRI, *Neuroimage*, 41, 3, 941–969

Marrelec, G., Benali, H., Ciuciu, P., Plgrini-Issac, M., and Poline, J.-B. (2003), Robust Bayesian estimation of the hemodynamic response function in event-related BOLD MRI using basic physiological information, *Human Brain Mapping*, 19, 1, 1–17

Ogawa, S., Lee, T., Kay, A., and Tank, D. (1990), Brain magnetic resonance imaging with contrast dependent on blood oxygenation, *Proceedings of the National Academy of Sciences of the United States of America*, 87, 24, 9868–9872

Operto, G., Bulot, R., Anton, J.-L., and Coulon, O. (2006), Anatomically informed convolution kernels for the projection of fMRI data on the cortical surface, in Proceedings 9th International Conference on Medical Image Computing and Computer Assised Intervention (Springer Verlag, Copenhaegen, Denmark), LNCS 4191, 300–307

Owens, J., Houston, M., Luebke, D., Green, S., Stone, J., and Phillips, J. (2008), Gpu computing, *Proceedings of the IEEE*, 96, 5, 879–899

Pinel, P., Thirion, B., Mriaux, S., Jobert, A., Serres, J., Le Bihan, D., et al. (2007), Fast reproducible identification and large-scale databasing of individual functional cognitive networks, *BMC Neurosci.*, 8, 1, 91

Risser, L., Vincent, T., Forbes, F., Idier, J., and Ciuciu, P. (2011), Min-max extrapolation scheme for fast estimation of 3D Potts field partition functions. application to the joint detection-estimation of brain activity in fMRI., *Journal of Signal Processing Systems*, 65, 3, 325–338

Thyreau, B., Thirion, B., Flandin, G., and Poline, J.-B. (2006), Anatomo-functional description of the brain: a probabilistic approach, in Proceedings 31th Proceedings of the International Conference on Acoustic, Speech and Signal Processing, volume V (Toulouse, France), volume V, 1109–1112

Tzourio-Mazoyer, N., Landeau, B., Papathanassiou, D., Crivello, F., Etard, O., Delcroix, N., et al. (2002), Automated anatomical labeling of activations in SPM using a macroscopic anatomical parcellation of the MNI MRI single-subject brain., *Neuroimage*, 15, 1, 273–89

Vincent, T., Ciuciu, P., and Thirion, B. (2008), Sensitivity analysis of parcellation in the joint detection-estimation of brain activity in fMRI, in 5th International Symposium on Biomedical Imaging (Paris, France), 568–571

Vincent, T., Risser, L., and Ciuciu, P. (2010), Spatially adaptive mixture modeling for analysis of within-subject fMRI time series, *IEEE Transactions on Medical Imaging*, 29, 4, 1059–1074

Vincent, T., Warnking, J., Villien, M., Krainik, A., Ciuciu, P., and Forbes, F. (2013), Bayesian Joint Detection-Estimation of cerebral vasoreactivity from ASL fMRI data, in 16th Proceedings Proc. MICCAI, LNCS Springer Verlag, volume 2 (Nagoya, Japan), volume 2, 616–623

Yan, L., Zhuo, Y., Ye, Y., Xie, S. X., An, J., Aguirre, G. K., et al. (2009), Physiological origin of low-frequency drift in blood oxygen level dependent (bold) functional magnetic resonance imaging (fMRI), *Magnetic Resonance in Medicine*, 61, 4, 819–827